Synthesis and Characterization of Polyaniline/Silica Doped with Camphorsulfonic Acid and Dodecylbenzylsulfonic Acid

Hsun-Tsing Lee, Shung-Jim Yang

Department of Chemical and Materials Engineering, Vanung University, Chung-Li 32061, Taiwan, Republic of China

Received 22 January 2007; accepted 19 October 2009
DOI 10.1002/app.31624
Published online 10 December 2009 in Wiley InterScience (www.interscience.wiley.com).

ABSTRACT: In this study, the effect of the dopant structure on the morphology, structure, optical absorption, conductivity, and thermal properties of conductive polyaniline (PAn)/silica (SiO_2) hybrids from a sol–gel process was first investigated. Camphorsulfonic acid (CSA) and dodecylbenzylsulfonic acid (DBSA) were used as the model acid dopants. The polaron absorption peaks of the CSA-doped PAn/SiO_2 (CSA–PAn/SiO_2) hybrids were redshifted compared with those of the DBSA–PAn/SiO_2 hybrids. This indicated that the doped PAn subchains of the CSA–PAn/SiO_2 hybrids had a more rigid conformation and longer conjugation length than those of DBSA–PAn/SiO_2 hybrids. Therefore, the CSA–PAn/SiO_2 hybrids were more conductive than the DBSA–PAn/SiO_2 hybrids with same SiO_2 contents. Moreover, the CSA–PAn/SiO_2 hybrids exhibited higher SiO_2 condensation degrees and thermal resistance than the DBSA–PAn/SiO_2 hybrids with same SiO_2 contents. In addition, the CSA–PAn/SiO_2 films exhibited a nonuniform globular morphology, whereas the DBSA–PAn/SiO_2 films showed an interconnected and rugged fibrillar one. © 2009 Wiley Periodicals, Inc. J Appl Polym Sci 116: 934–945, 2010

Key words: conducting polymers; silicas; thermal properties

INTRODUCTION

Polyaniline (PAn) is an important conducting polymer because of its electrochromic, antistatic, reversible doping/dedoping, and environmentally stable properties.[1–4] PAn has potential commercial applications in the electronics, optics, and anticorrosion industries. However, its mechanical and thermostability properties still need to be improved for use in harsh environments. In addition, PAn may be necessarily to adhere tightly to inorganic substrates, such as ceramics, metals, and glass, during application. Nevertheless, incompatibility between organic PAn and inorganic substrates would lead to a poor stability and durability for the applications. The preparation of a PAn/silica (SiO_2) organic/inorganic hybrid could solve these problems. Generally, organic/inorganic hybrids possess the processability properties of organic materials and excellent hardness and good adhesion of inorganic materials.[5,6] Uniform organic–inorganic hybrids are usually prepared from sol–gel processes. In the literature, only a few studies of conductive PAn/SiO_2 hybrids have been reported. They have included studies of the preparation methods, morphology, conductivity, and thermal properties.[5–11] There have been two processes for the preparation of PAn/SiO_2 hybrids discussed in the literature. One involves the electrochemical polymerization of aniline monomer in a porous sol–gel SiO_2.[7,8] The other is the chemical polymerization of aniline monomer followed by the condensation reaction of SiO_2 precursors.[5,6,9–11] These two processes give different types of PAn/SiO_2 hybrids. Much effort is still needed for an intimate investigation of conductive PAn/SiO_2 hybrids. The process adopted in this study was similar to the latter process.

For PAn/SiO_2 hybrids to be conductive, the PAn component must be doped in advance. PAn is different from other conjugated conducting polymers in that it can be doped to a conducting form without a change in the number of π electrons through protonation by exposure to an aqueous protonic acid solution.[12] The PAn of the ideal emeraldine base form contains alternating amine and imine repeat units (I, Scheme 1).[13,14] When PAn is doped by a protonic acid (H^+A^-), protonation occurs at the imine nitrogen sites to yield polysemiquinone (II, Scheme 1), in which the polarons delocalize along the chain.[13]

The acid dopants usually used for doping PAn are small molecular organic or inorganic acids. These acid dopants evaporate at room or higher

Correspondence to: H.-T. Lee (htlee@mail.vnu.edu.tw).
Contract grant sponsor: National Science Council of Republic of China.

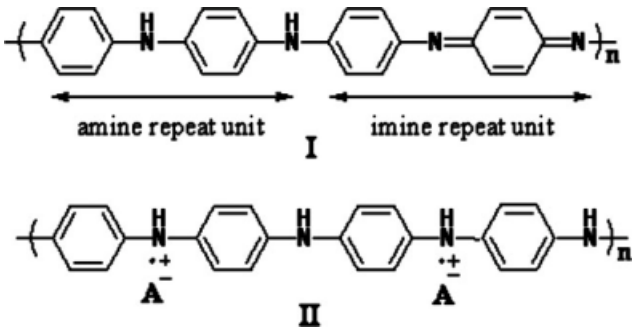

Scheme 1 Structure of the PAn before and after doping with a protonic acid.

temperature; this causes a conductivity depression of the acid-doped PAn.[1] This drawback can be overcome by the use of nonvolatile acid dopants, such as camphorsulfonic acid (CSA),[15,16] *p*-toluenesulfonic acid,[17] dodecylbenzylsulfonic acid (DBSA),[18,19] and polymeric acid.[20–23] CSA and DBSA were used as model acid dopants in this study. CSA has a bicyclic structure and a sulfonic acid group. DBSA has a hydrophilic sulfonic acid group at one end of the molecule and a hydrophobic long alkyl chain at the other end. Their structures are shown in Scheme 2.

An investigation of the effect of the acid-dopant structure on the morphology and properties of the hybrids is of prime importance for the illustration and utilization of these conductive PAn/SiO_2 hybrids. There is no literature concentrating on this investigation. Herein, the effects of the dopant structure on the morphology, structure, optical absorption, conductivity, and thermal properties of acid-doped PAn/SiO_2 hybrids are reported. Moreover, an understanding of the CSA-doped and DBSA-doped systems should also be applicable to systems with other nonvolatile protonic acid dopants.

EXPERIMENTAL

Materials

Tetraethoxysilane (TEOS; 98%), CSA (98%), and ammonium peroxydisulfate [$(NH_4)_2S_2O_8$, 98%] were purchased from Acros (Morris Plains, NJ). Hydrochloric acid (37%) and ammonium hydroxide (28%) were purchased from Nihon Shiyaku (Tokyo, Japan). *N*-methyl-2-pyrrolidinone (NMP; >99.5%) was obtained from FisherBiotech (Fair Lawn, NJ). DBSA (>96%) and oxalic acid (>99%) were purchased from Tokyo Kasei Kogyo (Tokyo, Japan) and Janssen

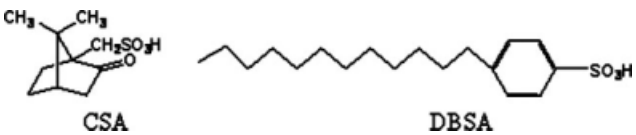

Scheme 2 Structure of CSA and DBSA.

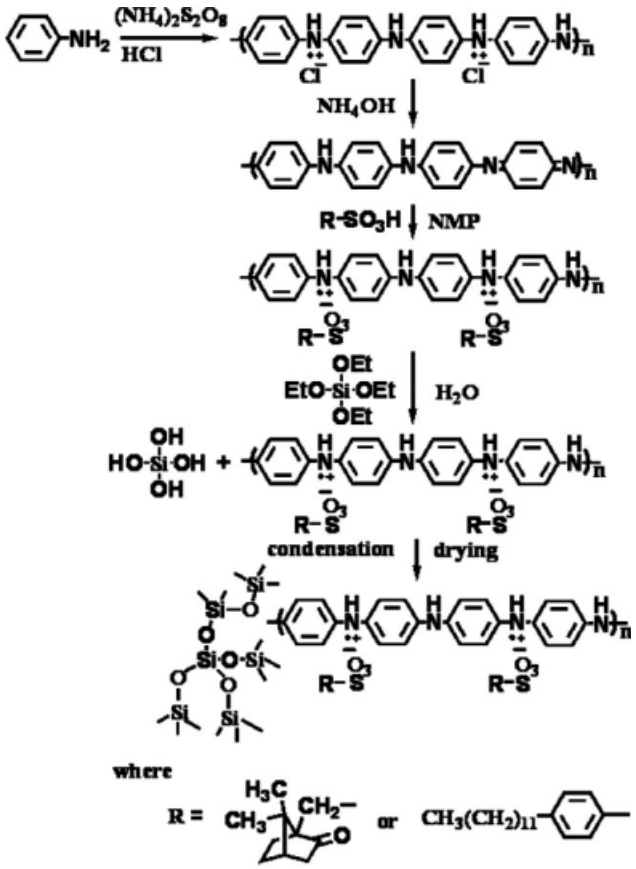

Scheme 3 Preparation process for the CSA–PAn/SiO_2 and DBSA–PAn/SiO_2 hybrids.

(Geel, Belgium), respectively. All of these reagents were synthetic grade and used as received. Aniline (99%) was obtained from Aldrich (St. Louis, MO) and purified by distillation *in vacuo* before use.

Synthesis of PAn

HCl-doped PAn powder was synthesized by the oxidative polymerization of aniline in 1*M* HCl with $(NH_4)_2S_2O_8$ as an oxidant. The details were described in our previous articles[1,24] and were similar to the method used by MacDiarmid et al.[25] The obtained HCl-doped PAn powder was converted to neutral PAn (emeraldine base) by treatment with 1*M* NH_4OH followed by drying under a dynamic vacuum. The neutral PAn was simply called PAn, and a flexible self-standing film was obtained when we cast the PAn solution in NMP.

Synthesis of the CSA–PAn/SiO_2 and DBSA–PAn/SiO_2 hybrids

The synthesis process for the CSA–PAn/SiO_2 and DBSA–PAn/SiO_2 hybrids is shown in Scheme 3. First, a PAn solution was obtained by the dissolution of 0.5 g of PAn powder in 30 mL of NMP. Another

CSA solution was obtained by the dissolution of 0.637 g of CSA powder in 5 mL of NMP. Subsequently, the PAn solution was mixed with the CSA solution to form a CSA-doped PAn (CSA–PAn) solution in NMP. For the PAn, half of the N atoms were in amine groups, and the other half were in imine groups. Only the imine groups could be doped by acid, so the maximum doping level of PAn was 0.5. Thus, the molar ratio of CSA to PAn used in this study was kept at 0.5 (the moles of PAn were based on the approximate repeat unit —C_6H_4NH—). Meanwhile, an SiO_2 precursor solution was obtained by the mixture of appropriate amounts of TEOS, deionized H_2O, and oxalic acid with a molar ratio of 10 : 60 : 0.7. The amounts of TEOS used were 60, 45, 30, 20, and 10 wt %, respectively, of the total amount of CSA, PAn, and TEOS used. The SiO_2 precursor solution was added to the CSA–PAn solution and stirred for 3 h at room temperature. Then, the solution mixture was poured into a Petri dish, kept at room temperature for 48 h, and then dried in an oven at 50°C for 96 h. Finally, the CSA–PAn/SiO_2 hybrid was obtained by drying under a dynamic vacuum at 60°C for 48 h. The DBSA–PAn/SiO_2 hybrids were obtained similarly. Both CSA–PAn/SiO_2 and DBSA–PAn/SiO_2 hybrids exhibited as brittle self-standing films. The neat SiO_2 powder was also prepared by the aforementioned procedure, except no CSA–PAn solution was added. This SiO_2 powder was prepared for comparison purposes.

During the preparation process for the hybrids and SiO_2, TEOS underwent the hydrolysis and condensation reactions depicted in the following.

Hydrolysis

$$\mathrm{Si(OEt)}_n + n\mathrm{H_2O} \rightarrow \mathrm{Si(OH)}_n + n\mathrm{EtOH}\ (n = 1\text{–}4)$$

Condensation

$$\equiv\mathrm{Si}\text{—}\mathrm{OH} + \mathrm{HO}\text{—}\mathrm{Si}\equiv \rightarrow \equiv\mathrm{Si}\text{—}\mathrm{O}\text{—}\mathrm{Si}\equiv + \mathrm{H_2O}$$

$$\equiv\mathrm{Si}\text{—}\mathrm{OH} + \mathrm{EtO}\text{—}\mathrm{Si}\equiv \rightarrow \equiv\mathrm{Si}\text{—}\mathrm{O}\text{—}\mathrm{Si}\equiv + \mathrm{EtOH}$$

The CSA–PAn/SiO_2 (45%) designation indicates a hybrid prepared from its components with 45 wt % TEOS (precursor of SiO_2). Other hybrids with the DBSA acid dopant or different amounts of TEOS used are designated in a similar way.

Characterization

An X-ray diffractometer (model ARL X'TRA, Thermo Electron Corp., Ecublens, Switzerland) was used to examine ordering in the specimens. Samples were ground and pressed into tablets for X-ray diffraction (XRD) examinations. The X-ray beam was Ni-filtered Cu Kα radiation from a sealed tube operated at 45 kV and 40 mA. Data were obtained in the 2θ range 3–40° with a 0.03° step and a fixed counting time of 2 s. A scanning electron microscope (model S-3000N, Hitachi, Ltd., Tokyo, Japan) was used to examine the morphologies of the specimens. A film of about 1 × 2 mm^2 was fixed on the sample holder with conductive adhesive tape and was then coated with a thin layer of gold to improve image resolution.

A Fourier transform infrared (FTIR) spectrophotometer (model Spectrum One, PerkinElmer Instruments, Norwalk, CT) with a resolution of 1 cm^{-1} was used to identify the chemical structures of the specimens. Samples were ground and mixed with KBr powder. The mixtures were then pressed into tablets for FTIR examinations. A ^{29}Si-NMR spectrometer [magic-angle spinning nuclear magnetic resonance (MAS NMR) spectrometer; model DSX-400, Bruker Optics, Ettlingen, Germany] was used to determine the relative population of the Si atom coordination states about the SiO_4 tetrahedra. These populations were quantified by Q^n peaks, where $Q^n = \mathrm{Si(OSi)}_n(\mathrm{OH})_{4-n}$. Tetramethylsilane was used as a reference for these solid-state NMR spectra. The complex NMR peaks were deconvoluted into component Gaussian peaks with peak separation and analysis software (PeakFit v4.0, AISN Software, Inc., Florence, OR).

An ultraviolet–visible (UV–vis) spectrophotometer (model UV-160, Shimadzu Corp., Kyoto, Japan) was used to measure the optical absorption of the thin solid films coated on glass plates. The electronic conductivities of the specimens were measured with the four-probe method under a dry nitrogen atmosphere at room temperature. The four probes were in line at an equal spacing of 1.6 mm (S). The samples were ground and pressed into tablets. During conductivity measurements, the four probes were put into intimate contact with the sample surface, and an appropriate constant current (I) in the range 10–60 mA was applied on the two outer probes. Then, the voltage (V) across the two inner probes was measured. The conductivity (σ) was calculated by $\sigma = I/(2\pi SV)$.[26] A thermogravimetric analyzer (model TGA-7, PerkinElmer Instruments) was used to measure the weight losses of the specimens at a heating rate of 10°C/min under a nitrogen stream. Before the temperature scan, each specimen was subject to a heating scan from room temperature to 100°C in the thermogravimetric analysis (TGA) furnace to remove any adsorbed moisture.

RESULTS AND DISCUSSION

Morphology

The XRD patterns of the CSA–PAn/SiO_2 and DBSA–PAn/SiO_2 hybrids with various SiO_2 contents and

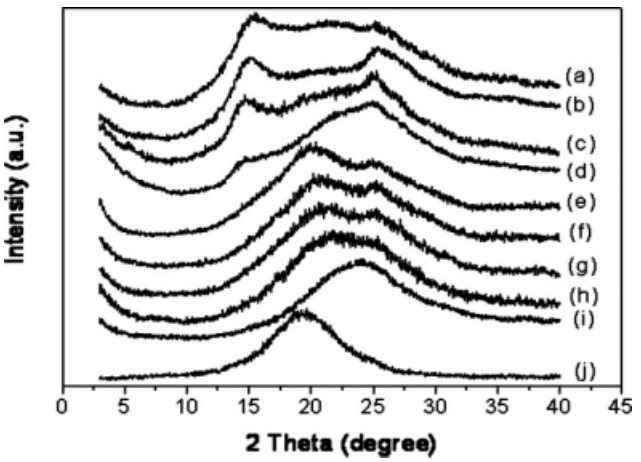

Figure 1 XRD patterns of the (a) CSA–PAn, (b) CSA–PAn/SiO_2 (30%), (c) CSA–PAn/SiO_2 (45%), (d) CSA–PAn/SiO_2 (60%), (e) DBSA–PAn, (f) DBSA–PAn/SiO_2 (30%), (g) DBSA–PAn/SiO_2 (45%), (h) DBSA–PAn/SiO_2 (60%), (i) SiO_2, and (j) PAn powders.

neat PAn and SiO_2 are shown in Figure 1. PAn exhibited a broad amorphous diffraction halo centered at a 2θ of about 19.3°. Similarly, SiO_2 showed another broad amorphous diffraction halo at a 2θ of about 23.7°. On the other hand, CSA–PAn showed a combined broad diffraction halo attached with two small broad peaks at 2θ's of about 15.7 and 25.3°. In addition, there was one unapparent broad peak between these two peaks. This XRD pattern indicated that CSA–PAn had heterogeneous phases with some short-range regularity (not crystallinity) in the subchains, which was ascribed to the interaction between CSA and PAn. A comparison between the pattern of CSA–PAn and the one of neat PAn indicated that the interaction between CSA and PAn created some special phases. However, the combined diffraction halos of the CSA–PAn/SiO_2 hybrids became narrower with increasing SiO_2 content. In addition, the attached broad peaks became smaller with increasing SiO_2 content. Therefore, the incorporation of SiO_2 interfered with the interaction between CSA and PAn and destroyed some original phases of CSA–PAn. This behavior was due to the interactions among CSA, PAn, and SiO_2.

Analogously, DBSA–PAn showed a combined broad diffraction halo attached with two small broad peaks at 2θ's of about 20.0 and 25.3°. A comparison between the pattern of DBSA–PAn and the one of neat PAn also indicated that the interaction between DBSA and PAn created some special phases in DBSA–PAn. The changes in the diffraction patterns of the DBSA–PAn/SiO_2 hybrids with increasing SiO_2 content were analogous to those of the CSA–PAn/SiO_2 hybrids.

Because CSA–PAn and DBSA–PAn exhibited differently shaped XRD patterns, it was hard to compare the packing orderliness of subchains between CSA–PAn and DBSA–PAn. However, large counterions, such as CSA^-, could have stopped the twist of PAn chains and kept the chains in a more expanded conformation.[27–29] Then, the expanded PAn chains would have coupled with each other, and the self-assembled CSA–PAn networks would be formed. CSA–PAn networks contribute to electron delocalization and conductivity.[27] Therefore, the conductivity of CSA–PAn was higher than that of DBSA–PAn, as illustrated later.

Scanning electron micrographs of the CSA–PAn/SiO_2 (45%), CSA–PAn/SiO_2 (30%), CSA–PAn, DBSA–PAn/SiO_2 (45%), DBSA–PAn/SiO_2 (30%), and DBSA–PAn films are shown in Figure 2. The CSA–PAn/SiO_2 (45%) and CSA–PAn/SiO_2 (30%) films showed a nonuniform globular morphology. On the other hand, the DBSA–PAn/SiO_2 (45%) and DBSA–PAn/SiO_2 (30%) films showed an interconnected and rugged fibrillar one. The CSA-based and DBSA-based hybrids exhibited different morphologies. Moreover, in the absence of SiO_2, the CSA–PAn film exhibited a morphology with plenty of small granular bulges, whereas the DBSA–PAn film showed a morphology with many fibrillar veins. The CSA–PAn and DBSA–PAn films exhibited different morphologies. Furthermore, the morphologies of the CSA–PAn and DBSA–PAn films were somewhat similar to those of CSA–PAn/SiO_2 and DBSA–PAn/SiO_2 hybrids, respectively. Meanwhile, the neat PAn film showed a smooth and featureless morphology.[30] Therefore, the morphology difference between the CSA–PAn/SiO_2 and DBSA–PAn/SiO_2 hybrids was due to a structural difference between CSA and DBSA. The mechanism may have been due to the three-dimensional structure of CSA and the two-dimensional structure and surfactant nature of DBSA.

Structure

The FTIR spectra of CSA–PAn/SiO_2 (45%), DBSA–PAn/SiO_2 (45%), PAn, SiO_2, CSA, and DBSA are shown in Figure 3. The main characteristic absorption peaks of PAn were 1585 cm^{-1} (C=C stretching of quinoid rings),[30] 1495 cm^{-1} (C=C stretching of benzenoid rings),[30] 1307 cm^{-1} (C—N stretching), and 1165 cm^{-1} (electronic-like absorption of N=Q=N,[31] where Q denotes the quinoid ring). When PAn was doped by CSA, as in the CSA–PAn/SiO_2 (45%) hybrid, the 1585-cm^{-1} peak shifted by 20 cm^{-1} to 1565 cm^{-1}, the 1495-cm^{-1} peak shifted by 22 cm^{-1} to 1473 cm^{-1}, the 1307-cm^{-1} peak shifted by 15 cm^{-1} to 1292 cm^{-1}, and the 1165-cm^{-1} peak shifted by 15 cm^{-1} to 1150 cm^{-1}. These redshift phenomena and a broad absorption at 2000–4000 cm^{-1} (free-carrier

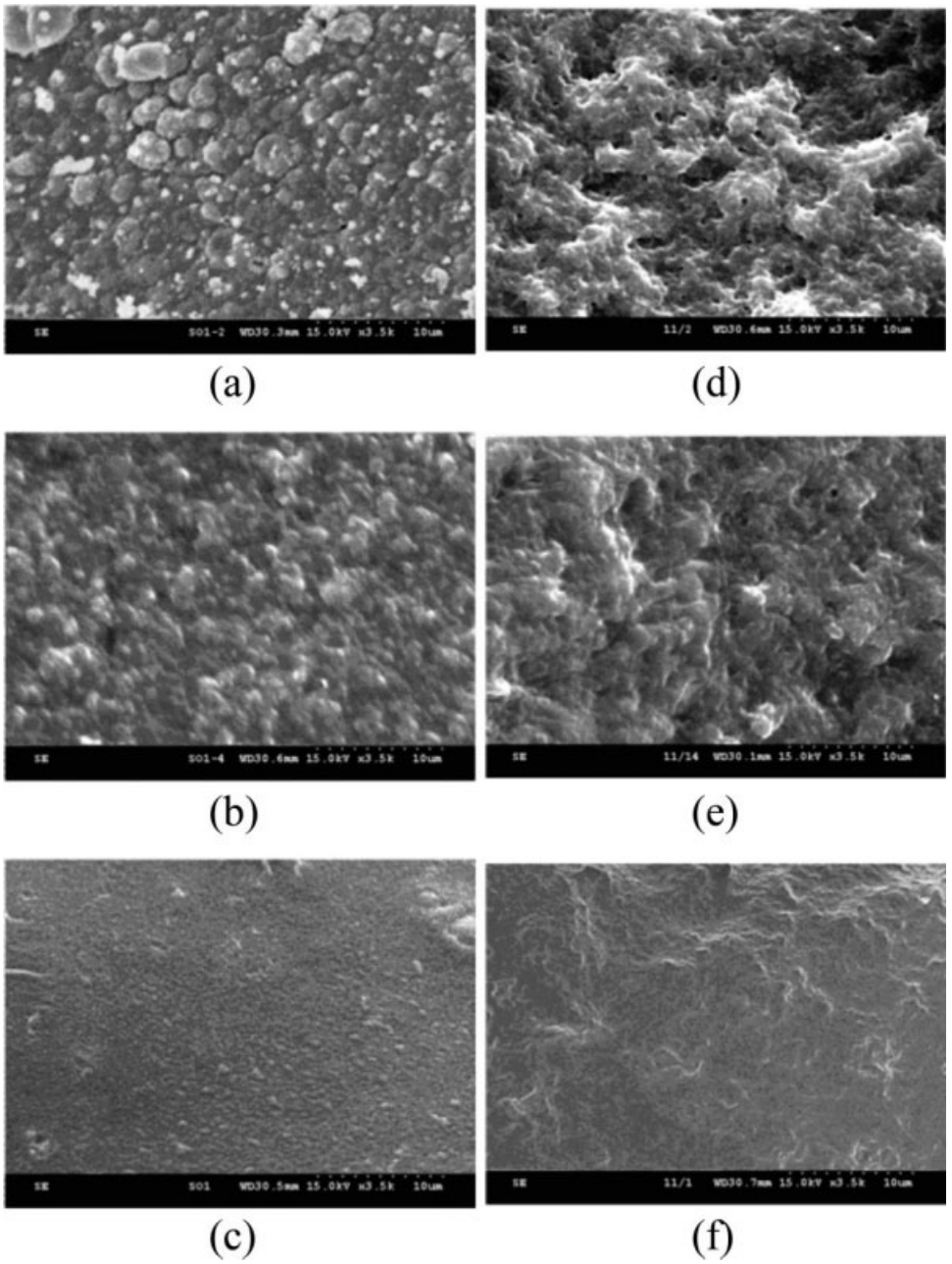

Figure 2 Scanning electron micrographs of the (a) CSA–PAn/SiO_2 (45%), (b) CSA–PAn/SiO_2 (30%), (c) CSA–PAn, (d) DBSA–PAn/SiO_2 (45%), (e) DBSA–PAn/SiO_2 (30%), and (f) DBSA–PAn films.

absorption)[32] for this hybrid indicated a doping phenomenon of PAn or an interaction between the —SO_3H group of CSA and the N=Q=N group of PAn. When PAn was doped by CSA, protonation occurred at the imine nitrogen sites to yield polysemiquinone, in which the polarons delocalized along the PAn chains. Another 1737-cm^{-1} peak for the hybrid was due to the C=O stretching of the CSA component.

Moreover, the SO_2 symmetric stretching for CSA at 1172 cm^{-1} shifted by 22 cm^{-1} to 1150 cm^{-1} and overlapped with the electronic-like absorption of doped N=Q=N in the CSA–PAn/SiO_2 hybrid. The S=O stretching for CSA at 1043 cm^{-1} shifted by 3 cm^{-1} to 1040 cm^{-1}. These two redshift phenomena of the CSA functional peaks also indicated the presence of interaction between CSA and PAn. In addition, the asymmetric stretching of the Si—O—Si group for the SiO_2 at 1083 cm^{-1} shifted by 43 cm^{-1} to 1040 cm^{-1} for the CSA–PAn/SiO_2 (45%) hybrid. This indicated the presence of hydrogen-bonding interaction between the Si—O—Si group of SiO_2 and the —NH group of PAn. Therefore, these IR spectra indicate the presence of hydrogen-bonding interactions among the Si—O—Si group of SiO_2, the —SO_3H group of CSA, and the —NH group of PAn.

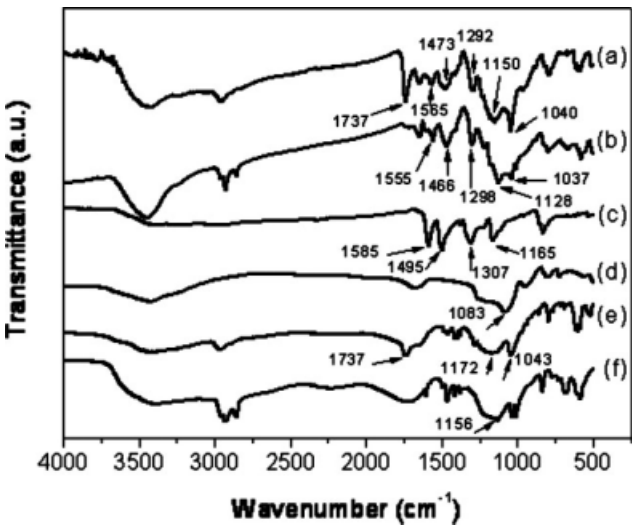

Figure 3 IR spectra of (a) CSA–PAn/SiO_2 (45%), (b) DBSA–PAn/SiO_2 (45%), (c) PAn, (d) SiO_2, (e) CSA, and (f) DBSA.

Similarly, the 1585-, 1495-, 1307-, and 1165-cm^{-1} peaks for neat PAn shifted to 1555, 1466, 1298, and 1128 cm^{-1}, respectively, for the DBSA–PAn/SiO_2 (45%) hybrid. Moreover, there was a broad absorption at 2000–4000 cm^{-1} for this hybrid; this was also observed for the previous CSA–PAn/SiO_2 (45%). Therefore, a doping phenomenon of PAn or an interaction between the —SO_3H group of DBSA and the N=Q=N group of PAn in the DBSA–PAn/SiO_2 (45%) hybrid was also observed. Moreover, the —SO_2— symmetric stretching for the —SO_3H group of DBSA at 1156 cm^{-1} shifted by 28 to 1128 cm^{-1} and overlapped with the electronic-like absorption of doped N=Q=N in the DBSA–PAn/SiO_2 hybrid. This redshift phenomenon of the DBSA functional peak also indicated the presence of an interaction between DBSA and PAn. In addition, the asymmetric stretching of the Si—O—Si group for SiO_2 at 1083 cm^{-1} shifted by 46 cm^{-1} to 1037 cm^{-1} for the DBSA–PAn/SiO_2 (45%) hybrid. These redshift phenomena indicated the presence of hydrogen0bonding interactions among the Si—O—Si group of SiO_2, the —SO_3H group of DBSA, and the —NH group of PAn. Therefore, the IR spectra confirmed the interactions among the acid-dopant, PAn, and SiO_2 components in the acid-doped PAn/SiO_2 hybrids.

Figure 4(A) shows the ^{29}Si MAS NMR spectra of the CSA–PAn/SiO_2 and DBSA–PAn/SiO_2 hybrids with various SiO_2 contents. The spectra showed three distinct peaks at about −92, −102, and −112 ppm, which corresponded to the Q^2, Q^3, and Q^4 structural units, respectively. Q^n represents the $Si(OSi)_n(OH)_{4-n}$ structural unit with n = 1–4. If TEOS was hydrolyzed and condensed completely, it would result in a solely Q^4 structure. Therefore, the SiO_2 in these hybrids was not condensed completely. The complex NMR peaks of each hybrid were deconvoluted into component peaks. A representative deconvolution result for the CSA–PAn/SiO_2 (30%) hybrid is shown in Figure 4(B). The calculated relative areas under the Q^n peaks and the area ratio of the Q^4 peak to the Q^3 one (Q^4/Q^3) for each hybrid are listed in Table I. SiO_2 in these hybrids had major structural units of Q^3 and Q^4. Moreover, Q^4/Q^3 increased with increasing SiO_2 content for both the CSA–PAn/SiO_2 and DBSA–PAn/SiO_2 hybrids. For example, Q^4/Q^3 of DBSA–PAn/SiO_2 (30%) was 1.00, whereas that of DBSA–PAn/SiO_2 (45%) was 1.04; meanwhile, Q^4/Q^3 of CSA–PAn/SiO_2 (30%) was 1.07, whereas that of CSA–PAn/SiO_2 (45%) was 1.18. Theoretically, the hybrid with a larger Q^4/Q^3 value would have a higher condensation degree of the SiO_2 component. Therefore, the introduction of more SiO_2 or less conductive PAn into the hybrid resulted in a higher degree of three-dimensional network

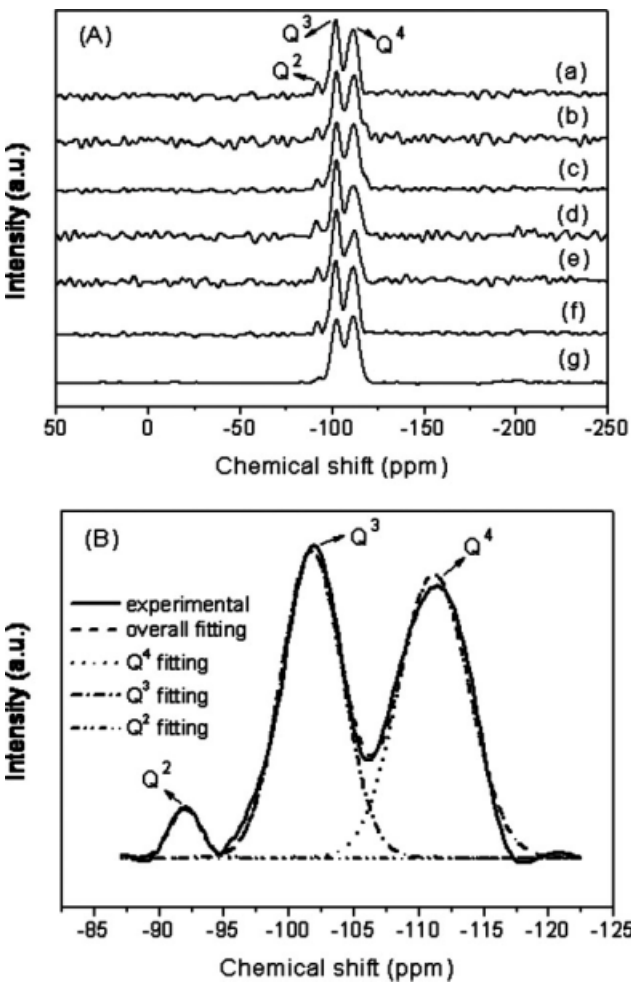

Figure 4 (A) ^{29}Si MAS NMR spectra of (a) CSA–PAn/SiO_2 (30%), (b) CSA–PAn/SiO_2 (45%), (c) CSA–PAn/SiO_2 (60%), (d) DBSA–PAn/SiO_2 (30%), (e) DBSA–PAn/SiO_2 (45%), (f) DBSA–PAn/SiO_2 (60%), and (g) SiO_2. (B) Representative deconvolution results for the CSA–PAn/SiO_2 (30%) hybrid.

TABLE I
Relative Areas Under the Q^n Peaks and Area Ratios of the Q^4 Peak to the Q^3 Peak (Q^4/Q^3) for the CSA–PAn/SiO_2 and DBSA–PAn/SiO_2 Hybrids

Hybrid	Q^1 (%)	Q^2 (%)	Q^3 (%)	Q^4 (%)	Q^4/Q^3
CSA–PAn/SiO_2 (10%)	—	7.6	46.0	46.4	1.01
CSA–PAn/SiO_2 (20%)	—	4.1	46.8	49.1	1.05
CSA–PAn/SiO_2 (30%)	—	3.8	46.4	49.8	1.07
CSA–PAn/SiO_2 (45%)	—	3.8	44.1	52.1	1.18
CSA–PAn/SiO_2 (60%)	—	3.1	44.0	52.9	1.20
DBSA–PAn/SiO_2 (10%)	—	8.3	47.0	44.7	0.95
DBSA–PAn/SiO_2 (20%)	—	8.0	46.7	45.3	0.97
DBSA–PAn/SiO_2 (30%)	—	7.8	46.0	46.2	1.00
DBSA–PAn/SiO_2 (45%)	—	4.3	46.9	48.8	1.04
DBSA–PAn/SiO_2 (60%)	—	3.8	45.6	50.6	1.11
SiO_2	—	1.9	43.7	54.4	1.24

structures for the SiO_2. This was because the silanol groups in the region with a higher silicic acid (SiO_2 sol) concentration had more opportunity to undergo condensation reactions, as indicated by the highest Q^4/Q^3 value for the pure SiO_2 compound.

In other words, the incorporation of more acid-doped PAn into the hybrid enhanced the hydrogen-bonding interactions among the acid dopant, PAn, and SiO_2 during the whole sol–gel process. The strong hydrogen-bonding interactions effectively prevented silicic acid from aggregating for complete condensation.[9] This led, to a less degree, to the three-dimensional network structure and a lower Q^4/Q^3 value for the SiO_2 component of hybrids with higher acid-doped PAn content. The variation of Q^4/Q^3 values with SiO_2 or acid-doped PAn content in the hybrids indicated that there was a strong interaction or some miscibility between the acid-doped PAn and SiO_2. The reason was that if the two components aggregated separately, the Q^4/Q^3 values would be independent of the acid-doped PAn or SiO_2 contents of the hybrids.

Moreover, the Q^4/Q^3 values of the DBSA–PAn/SiO_2 hybrids were lower than those of CSA–PAn/SiO_2 hybrids with same SiO_2 contents. This was probably due to the surfactant characteristic of DBSA. That is, the presence of DBSA improved the compatibility between the acid-doped PAn and silicic acid. This effectively prevented silicic acid from aggregating for complete condensation. Therefore, the Q^4/Q^3 values of the DBSA–PAn/SiO_2 hybrids were lower than those of the CSA–PAn/SiO_2 hybrids with the same SiO_2 contents. Also, the pH difference between the DBSA–PAn/SiO_2 and CSA–PAn/SiO_2 sols was probably another factor in the Q^4/Q^3 difference. First, Figure 5 shows that the pH values of the aqueous DBSA solutions were higher than those of the aqueous CSA solutions. Consequently, the pH values of the DBSA–PAn/SiO_2 sols [2.30 for DBSA–PAn/SiO_2 (45%)] were higher than those of the CSA–PAn/SiO_2 sols [1.95 for CSA–PAn/SiO_2 (45%)]. The SiO_2 sol in a circumstance with a higher pH value exhibited a lower condensation rate. Therefore, the Q^4/Q^3 values of the DBSA–PAn/SiO_2 hybrids were lower than those of the CSA–PAn/SiO_2 hybrids.

Optical absorption and conductivity

The UV–vis spectra of CSA–PAn/SiO_2 and DBSA–PAn/SiO_2 hybrids with various SiO_2 contents and PAn are shown in Figure 6. Their corresponding absorption peaks are listed in Table II. The UV–vis spectrum of PAn exhibited two absorption peaks at 331 and 639 nm, which were due to the π–π^* transition of benzenoid rings and the exciton absorption of quinoid rings, respectively.[33,34] On the other hand, CSA–PAn had three absorption peaks at 350, 436, and 856 nm. The first arose from the aforementioned π–π^* transition of the benzenoid rings in PAn. The second and third were attributed to the

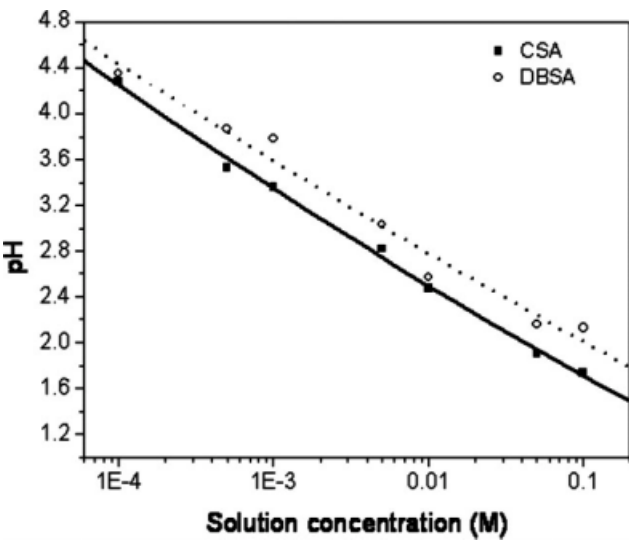

Figure 5 pH values of aqueous CSA and DBSA solutions with various concentrations.

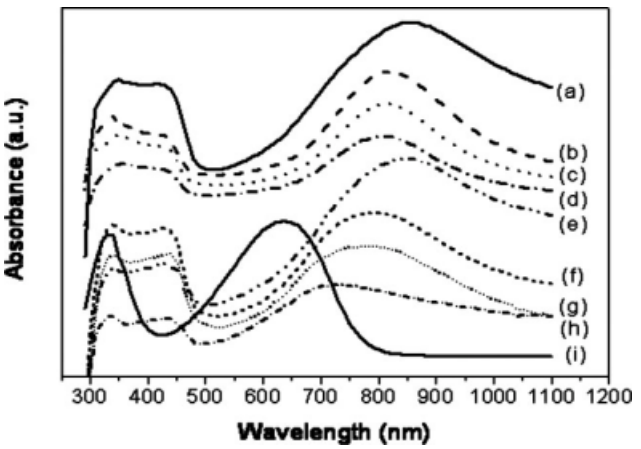

Figure 6 UV–vis spectra of the (a) CSA–PAn, (b) CSA–PAn/SiO_2 (30%), (c) CSA–PAn/SiO_2 (45%), (d) CSA–PAn/SiO_2 (60%), (e) DBSA–PAn, (f) DBSA–PAn/SiO_2 (30%), (g) DBSA–PAn/SiO_2 (45%), (h) DBSA–PAn/SiO_2 (60%). and (i) PAn films.

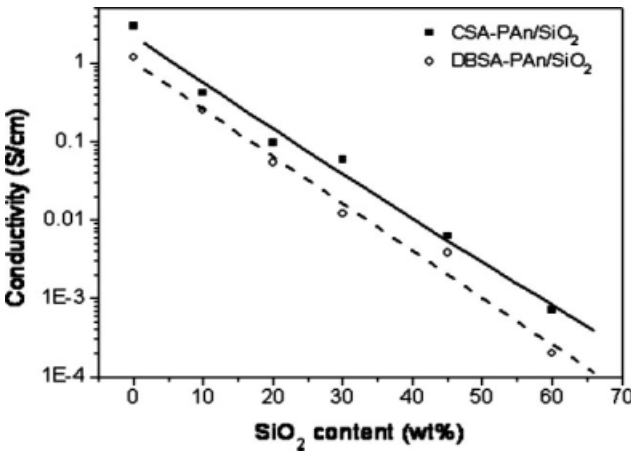

Figure 7 Electronic conductivities of CSA–PAn/SiO_2 and DBSA–PAn/SiO_2 hybrids with various SiO_2 contents.

formation of polarons in PAn.[35,36] The first and second often overlapped to form a flat or distorted single peak, which indicated a high level of doping.[36] Similarly, DBSA–PAn also had three absorption peaks at 342, 430, and 853 nm.

The effect of the SiO_2 component on the polaron peaks of doped PAn was observed from the UV–vis spectra. The polaron absorption peaks centered at 806–852 nm of the CSA–PAn/SiO_2 hybrids exhibited a blueshift phenomenon compared with that of CSA–PAn. The blueshift phenomenon was more significant with higher SiO_2 contents. This indicated that the stronger bonding strength of CSA–PAn/SiO_2 appeared after the incorporation of SiO_2, which restricted the delocalization of polarons or electrons along the PAn subchains. Similarly, polaron peaks for the blends of conductive PAn with other nonconductive polymers have also shown blueshift phenomena[37,38] compared with that of neat conductive PAn. The reason for the blueshift of the polaron absorption peak of CSA–PAn in the CSA–PAn/SiO_2 hybrids was the presence of strong hydrogen-bonding interaction between SiO_2 and CSA–PAn. Analogously, the polaron absorption peaks of the DBSA–PAn/SiO_2 hybrids also exhibited more significant blueshift phenomena with increasing SiO_2 content.

In addition, the wavelength of the polaron absorption peak for the CSA–PAn film was larger than that for DBSA–PAn. Thus, the interaction between PAn and CSA was stronger than that between PAn and DBSA. Similarly, the wavelengths of polaron absorption peaks for the CSA–PAn/SiO_2 hybrids were larger than those for the DBSA–PAn/SiO_2 hybrids with same SiO_2 contents. Therefore, the conjugation lengths of CSA–PAn/SiO_2 hybrids and CSA–PAn were longer than those of the DBSA–PAn/SiO_2 hybrids and DBSA–PAn, respectively. This was caused by the higher acidity of CSA than DBSA, as previously shown in Figure 5.

Figure 7 shows the electronic conductivities of CSA–PAn/SiO_2 and DBSA–PAn/SiO_2 hybrids with various SiO_2 contents. The conductivities of both the CSA–PAn/SiO_2 and DBSA–PAn/SiO_2 hybrids decreased with increasing SiO_2 content. This was because the incorporation of SiO_2 interfered with the interaction between the acid dopant and PAn and thereby destroyed some original phases or conjugation lengths of acid-doped PAn, as revealed in the previous XRD patterns and UV–vis spectra. Moreover, the insulation effect of the nonconductive SiO_2 component also lowered the conductivities of the hybrids.

Moreover, the conductivities of the hybrids were also influenced by the acid-dopant structures. For

TABLE II
UV–Vis Absorption Peaks for the CSA–PAn/SiO_2 and DBSA–PAn/SiO_2 Hybrids

Hybrid	Absorption peaks (nm)		
CSA–PAn	350	436	856
CSA–PAn/SiO_2 (10%)	342	435	852
CSA–PAn/SiO_2 (20%)	342	432	827
CSA–PAn/SiO_2 (30%)	342	430	818
CSA–PAn/SiO_2 (45%)	342	430	816
CSA–PAn/SiO_2 (60%)	342	430	806
DBSA–PAn	342	430	853
DBSA–PAn/SiO_2 (10%)	342	430	846
DBSA–PAn/SiO_2 (20%)	342	430	825
DBSA–PAn/SiO_2 (30%)	342	430	794
DBSA–PAn/SiO_2 (45%)	342	430	788
DBSA–PAn/SiO_2 (60%)	342	430	725
PAn	331	—	639

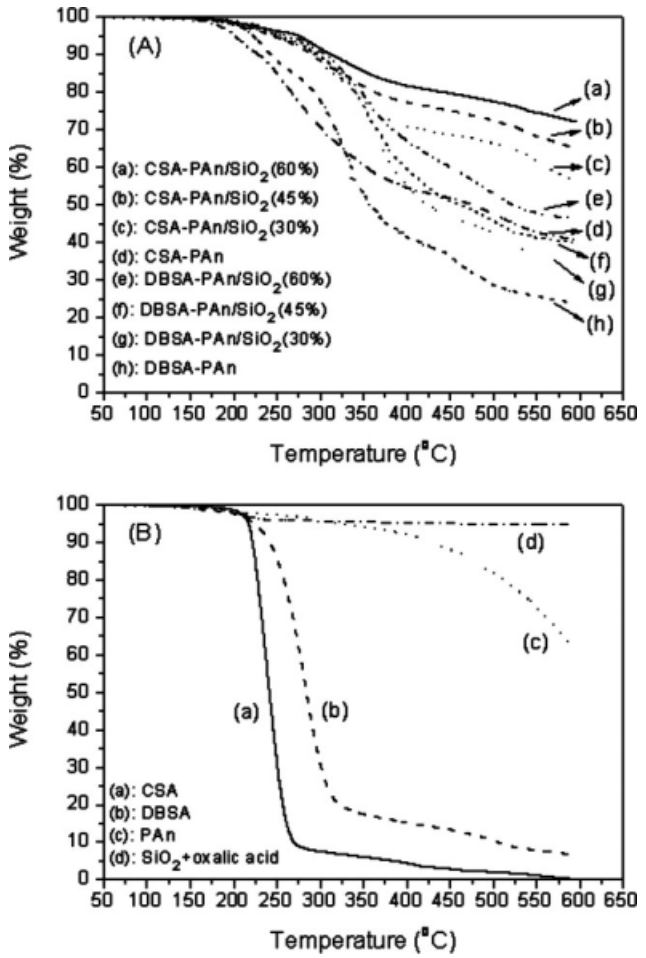

Figure 8 (A) TGA curves of (a) CSA–PAn/SiO_2 (60%), (b) CSA–PAn/SiO_2 (45%), (c) CSA–PAn/SiO_2 (30%), (d) CSA–PAn, (e) DBSA–PAn/SiO_2 (60%), (f) DBSA–PAn/SiO_2 (45%), (g) DBSA–PAn/SiO_2 (30%) and (h) DBSA–PAn films; (B) TGA curves of (a) CSA, (b) DBSA, (c) PAn and (d) SiO_2 containing 4.05 wt % oxalic acid.

example, the conductivities of the CSA–PAn/SiO_2 (45%) and DBSA–PAn/SiO_2 (45%) hybrids were 6.3 $\times$ 10^{-3} and 3.8 $\times$ 10^{-3} S/cm, respectively. The former was higher than the latter. This was because CSA was more acidic than DBSA, as previously shown in Figure 5. The PAn component doped by a stronger acid had a greater conjugation length and a higher conductivity.

Thermal properties

Figure 8(A) shows the TGA thermograms of CSA–PAn/SiO_2 and DBSA–PAn/SiO_2 hybrids with various SiO_2 contents. Figure 8(B) shows the TGA thermograms of CSA, DBSA, PAn, and SiO_2 containing 4.05 wt % oxalic acid. The small amount of oxalic acid was used to promote the hydrolysis and condensation reactions of SiO_2. The weight loss of the SiO_2 powder was mainly due to the decomposition of inner oxalic acid when heating was done in the range 160–250°C. When heating was done above 250°C, there was nearly no more weight loss of SiO_2. Therefore, SiO_2 was expected to contribute to the thermal resistance of the hybrids. There were limited weight losses for all of the hybrids when heating was done below 200°C. When the hybrids were heated above 200°C, there were two stages of weight losses: from 200 to 350°C and from 350 to 600°C. Meanwhile, the neat CSA and DBSA decomposed profoundly above 200°C and almost completely below 350°C. On the other hand, the neat PAn decomposed gradually when heating was done in the range 200–350°C and decomposed evidently when heating was done above 350°C. Therefore, the weight losses of all of the hybrids were mainly caused by the decompositions of the acid-dopant and PAn components when the hybrids were heated below and above 350°C, respectively.

Generally, the temperature at which weight loss reaches 5% is assigned to be the decomposition temperature (T_d). Analogously, T_{25} represents the temperature at which the weight loss of the hybrid reaches 25%. Both T_d and T_{25} increased with SiO_2 content, as shown in Figure 9. The enhancement of thermal resistance through the incorporation of SiO_2 was more significant, as indicated by the T_{25} curve. That is, the hybrid with a higher SiO_2 content exhibited a higher thermal resistance and had a weightier residue after it was heated to 600°C. This was due to the high thermal resistance of the SiO_2 component.

In addition, the acid–dopant structure influenced the thermal resistance of the hybrids. The rising trend in T_d or T_{25} with SiO_2 content was more significant for the CSA–PAn/SiO_2 hybrids than for

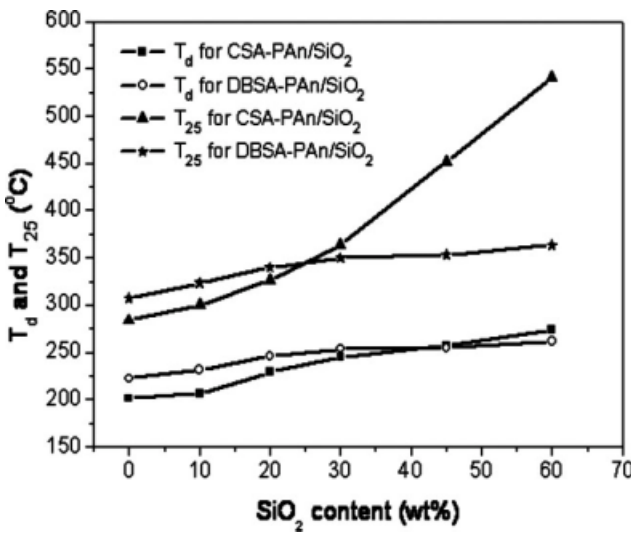

Figure 9 T_d and T_{25} values of CSA–PAn/SiO_2 and DBSA–PAn/SiO_2 hybrids with various SiO_2 contents.

TABLE III
Compositions of the CSA–PAn/SiO_2 and DBSA–PAn/SiO_2 Hybrids

Hybrid	Component	Feed composition (g)	Hybrid composition (g)
CSA–PAn	CSA	0.637	0.637 (56.02 wt %)
	PAn	0.5	0.5 (43.98 wt %)
CSA–PAn/SiO_2 (30%)	CSA	0.637	0.637 (48.63 wt %)
	PAn	0.5	0.5 (38.17 wt %)
	TEOS (SiO_2)[a]	0.487	0.152[b] (11.60 wt %)
	Oxalic acid	0.021	0.021 (1.60 wt %)
CSA–PAn/SiO_2 (45%)	CSA	0.637	0.637 (43.48 wt %)
	PAn	0.5	0.5 (34.13 wt %)
	TEOS (SiO_2)[a]	0.930	0.289[b] (19.73 wt %)
	Oxalic acid	0.039	0.039 (2.66 wt %)
CSA–PAn/SiO_2 (60%)	CSA	0.637	0.637 (36.67 wt %)
	PAn	0.5	0.5 (28.79 wt %)
	TEOS (SiO_2)[a]	1.706	0.528[b] (30.40 wt %)
	Oxalic acid	0.072	0.072 (4.14 wt %)
DBSA–PAn	DBSA	0.895	0.895 (64.16 wt %)
	PAn	0.5	0.5 (35.84 wt %)
DBSA–PAn/SiO_2 (30%)	DBSA	0.895	0.895 (55.66 wt %)
	PAn	0.5	0.5 (31.09 wt %)
	TEOS (SiO_2)[a]	0.598	0.188[b] (11.69 wt %)
	Oxalic acid	0.025	0.025 (1.55 wt %)
DBSA–PAn/SiO_2 (45%)	DBSA	0.895	0.895 (49.75 wt %)
	PAn	0.5	0.5 (27.79 wt %)
	TEOS (SiO_2)[a]	1.141	0.356[b] (19.79 wt %)
	Oxalic acid	0.048	0.048 (2.67 wt %)
DBSA–PAn/SiO_2 (60%)	DBSA	0.895	0.895 (41.94 wt %)
	PAn	0.5	0.5 (23.43 wt %)
	TEOS (SiO_2)[a]	2.092	0.651[b] (30.51 wt %)
	Oxalic acid	0.088	0.088 (4.12 wt %)

[a] TEOS for the feed and SiO_2 for the hybrid.
[b] The weight of SiO_2 in the hybrid was calculated from the moles of TEOS (i.e., moles of SiO_2) and the molar percentages of Q^2 [molecular weight (M_w) = 78.0 g/mol], Q^3 (M_w = 69.0 g/mol), and Q^4 (M_w = 60.0 g/mol) listed in Table I.

DBSA–PAn/SiO_2 (Fig. 9). Moreover, the compositions of CSA–PAn/SiO_2 and DBSA–PAn/SiO_2 hybrids with various SiO_2 contents are listed in Table III for calculating the expected residues of these hybrids after they were heated to 600°C. The expected and actual residues of the CSA–PAn/SiO_2 and DBSA–PAn/SiO_2 hybrids and their components after heating to 600°C are compared in Table IV. The

TABLE IV
Residues of the CSA–PAn/SiO_2 and DBSA–PAn/SiO_2 Hybrids and Their Components from the TGA Measurements

Hybrid	Expected residue at 600°C (*A*)[a]	Residue at 600°C from TGA measurement (*B*)	Difference between *A* and *B*
CSA		0 wt %	
DBSA		6.6 wt %	
PAn		60.7 wt %	
SiO_2		98.7 wt %[b]	
Oxalic acid		0 wt %	
CSA–PAn	26.7 wt %	40.7 wt %	14.0 wt %
CSA–PAn/SiO_2 (30%)	34.6 wt %	56.7 wt %	22.1 wt %
CSA–PAn/SiO_2 (45%)	40.2 wt %	65.0 wt %	24.8 wt %
CSA–PAn/SiO_2 (60%)	47.5 wt %	72.3 wt %	24.8 wt %
DBSA–PAn	26.0 wt %	23.9 wt %	−2.1 wt %
DBSA–PAn/SiO_2 (30%)	34.1 wt %	36.3 wt %	2.2 wt %
DBSA–PAn/SiO_2 (45%)	39.7 wt %	40.1 wt %	0.4 wt %
DBSA–PAn/SiO_2 (60%)	47.1 wt %	46.7 wt %	−0.4 wt %

[a] Calculated from the weight percentage compositions in Table III and the residues of the neat components after heating to 600°C for the TGA measurement.
[b] Exclusive of inner oxalic acid.

neat CSA and oxalic acid in SiO_2 decomposed and were lost completely before they were heated to 600°C. The neat DBSA, PAn, and SiO_2 (exclusive of inner oxalic acid) had residues of 6.6, 60.7, and 98.7 wt %, respectively, after they were heated to 600°C. Therefore, when CSA–PAn was heated to 600°C, the CSA component was expected to disappear completely, whereas the PAn component (43.98 wt % originally) was expected to remain at 26.7 wt %. However, the actual residue of CSA–PAn from TGA measurement was 40.7 wt %. The actual residue of CSA–PAn was higher than the expected one with a difference of 14.0 wt %. On the other hand, the expected and actual residues of DBSA–PAn were nearly the same. Similarly, after the CSA–PAn/SiO_2 (45%) hybrid was heated to 600°C, the PAn (34.13 wt % originally) and SiO_2 (19.73 wt % originally) components were expected to remain at 20.7 and 19.5 wt %, respectively. Therefore, the expected residue of the CSA–PAn/SiO_2 (45%) hybrid was 40.2 wt %. However, the actual residue of the CSA–PAn/SiO_2 (45%) hybrid from TGA measurement was 65.3 wt %. The actual residue of CSA–PAn/SiO_2 (45%) was higher than the expected one, with a difference of 25.1 wt %. Other CSA–PAn/SiO_2 hybrids with different SiO_2 contents exhibited similar characteristics. On the other hand, the expected and actual residues of the DBSA–PAn/SiO_2 hybrids were nearly the same. Analyses of the differences between the expected and actual residues of the CSA–PAn, DBSA–PAn, CSA–PAn/SiO_2, and DBSA–PAn/SiO_2 hybrids provided some interesting observations. That is, the thermal resistance of PAn was enhanced by the presence of CSA but was almost unaffected by DBSA. The different outcome in the enhancement of thermal resistance by the incorporation of CSA or DBSA was probably due to the stronger interaction of PAn with CSA than with DBSA.

CONCLUSIONS

Conductive CSA–PAn/SiO_2 and DBSA–PAn/SiO_2 hybrids were prepared from a sol–gel process. The CSA–PAn/SiO_2 films exhibited a nonuniform globular morphology, whereas the DBSA–PAn/SiO_2 films showed an interconnected and rugged fibrillar one. Moreover, the polaron absorption peaks of the CSA–PAn/SiO_2 hybrids were redshifted compared with those of the DBSA–PAn/SiO_2 hybrids. This indicated that the doped PAn subchains of the CSA–PAn/SiO_2 hybrids had a more rigid conformation and a longer conjugation length than those of the DBSA–PAn/SiO_2 hybrids. Therefore, the CSA–PAn/SiO_2 hybrids were more conductive than the DBSA–PAn/SiO_2 hybrids with the same SiO_2 contents. Meanwhile, the conductivities of both the CSA–PAn/SiO_2 and DBSA–PAn/SiO_2 hybrids decreased with increasing SiO_2 content. This was due to the conformational hindrance and insulating property of the SiO_2 network chains. Also, the CSA–PAn/SiO_2 hybrids exhibited a higher SiO_2 condensation degree and thermal resistance than the DBSA–PAn/SiO_2 hybrids with same SiO_2 contents. Consequently, the CSA–PAn/SiO_2 hybrids were better than the DBSA–PAn/SiO_2 hybrids in terms of application.

References

1. Chen, S. A.; Lee, H. T. Macromolecules 1995, 28, 2858.
2. Genies, E. M.; Lapkowski, M. Synth Met 1988, 24, 61.
3. Chao, D.; Lu, X.; Chen, J.; Zhao, X.; Wang, L.; Zhang, W.; Wei, Y. J Polym Sci Part A: Polym Chem 2006, 44, 477.
4. Angelopoulos, M.; Ray, A.; MacDiarmid, A. G.; Epstein, A. J. Synth Met 1987, 21, 21.
5. Wei, Y.; Yeh, J. M.; Jin, D.; Jia, X.; Wang, J.; Jang, G. W.; Chen, C.; Gumbs, R. W. Chem Mater 1995, 7, 969.
6. Wang, Y.; Wang, X.; Li, J.; Mo, Z.; Zhao, X.; Jing, X.; Wang, F. Adv Mater 2001, 13, 1582.
7. Widera, J.; Kijak, A. M.; Ca, D. V.; Pacey, G. E.; Taylor, R. T.; Perfect, H.; Cox, J. A. Electrochim Acta 2005, 50, 1703.
8. Verghese, M. M.; Ramanathan, K.; Ashraf, S. M.; Kamalasanan, M. N.; Malhotra, B. D. Chem Mater 1996, 8, 822.
9. Wang, Q.; Liu, N.; Wang, X.; Li, J.; Zhao, X.; Wang, F. Macromolecules 2003, 36, 5760.
10. de Azevedo, W. M.; Brondani, D. J. J Non-Cryst Solids 2001, 296, 224.
11. Jang, S. H.; Han, M. G.; Im, S. S. Synth Met 2000, 110, 17.
12. Hwang, G. W.; Wu, K. Y.; Hua, M. Y.; Lee, H. T.; Chen, S. A. Synth Met 1998, 92, 39.
13. MacDiarmid, A. G.; Epstein, A. J. Faraday Discuss Chem Soc 1989, 88, 317.
14. Asturias, G. E.; MacDiarmid, A. G.; McCall, R. P.; Epstein, A. J. Synth Met 1989, 29, 157.
15. Nascimento, G. M.; Constantino, V. R. L.; Landers, R.; Temperini, M. L. A. Polymer 2006, 47, 6131.
16. Cruz-Silva, R.; Ruiz-Flores, C.; Arizmendi, L.; Romero-Garcia, J.; Arias-Marin, E.; Moggio, I.; Castillon, F. F.; Farias, M. H. Polymer 2006, 47, 1563.
17. Hosseini, S. H.; Dabiri, M.; Ashrafi, M. Polym Int 2006, 55, 1081.
18. Souza, F. G.; Sirelli, L.; Michel, R. C.; Soares, B. G.; Herbst, M. H. J Appl Polym Sci 2006, 102, 535.
19. Hino, T.; Taniguchi, S.; Kuramoto, N. J Polym Sci Part A: Polym Chem 2006, 44, 718.
20. Kang, Y.; Lee, M. H.; Rhee, S. B. Synth Met 1992, 52, 319.
21. Lapkowski, M. Synth Met 1993, 55, 1558.
22. Angelopoulos, M.; Patel, N.; Saraf, R. Synth Met 1993, 55, 1552.
23. Lin, D. S.; Chou, C. T.; Chen, Y. W.; Kuo, K. T.; Yang, S. M. J Appl Polym Sci 2006, 100, 4023.
24. Lee, H. T.; Chuang, K. R.; Chen, S. A.; Wei, P. K.; Hsu, J. H.; Fann, W. Macromolecules 1995, 28, 7645.
25. Asturias, G. E.; MacDiarmid, A. G.; McCall, R. P.; Epstein, A, J. Synth Met 1989, 29, 157.
26. Elsenbaumer, R. L.; Shacklette, L. W. In Handbook of Conducting Polymers; Skotheim, T. A., Ed.; Marcel Dekker: New York, 1986; p 224.
27. Long, Y.; Chen, Z.; Wang, N.; Zhang, Z.; Wan, M. Phys B: Condens Matter 2003, 325, 208.
28. Cao, Y.; Smith, P.; Heeger, A. J. Synth Met 1992, 48, 91.

29. Li, W.; Wan, M. Synth Met 1998, 92, 121.
30. Chen, S. A.; Lee, H. T. Macromolecules 1993, 26, 3254.
31. Salaneck, W. R.; Liedberg, B.; Inganas, O.; Erlandsson, R.; Lundstrom, I.; MacDiarmid, A. G.; Halpern, M.; Somasiri, N. L. D. Mol Cryst Liq Cryst 1985, 121, 191.
32. Tourillon, G. In Handbook of Conducting Polymers; Skotheim, T. A., Ed.; Marcel Dekker: New York, 1986; p 318.
33. Lu, F. L.; Wudl, F.; Nowak, M.; Heeger, A. J. J Am Chem Soc 1986, 108, 8311.
34. Stafstrom, S.; Bredas, J. L.; Epstein, A. J.; Woo, H. S.; Tanner, D. B.; Huang, W. S.; MacDiarmid, A. G. Phys Rev Lett 1987, 59, 1464.
35. Yin, W.; Ruckenstein, E. Synth Met 2000, 108, 39.
36. Moulton, S. E.; Innis, P. C.; Kane-Maguire, L. A. P.; Ngamna, O.; Wallace, G. G. Curr Appl Phys 2004, 4, 402.
37. Rodrigues, P. C.; Lisboa-Filho, P. N.; Mangrich, A. S.; Akcelrud, L. Polymer 2005, 46, 2285.
38. Kulszewicz-Bajer, I.; Zagorska, M.; Rozalska, I. Synth Met 2001, 119, 69.